Geochemical evidence for exhumation of eclogite via serpentinite channels in ocean-continent subduction zones

Ulyana Horodyskyj*, Cin-Ty A. Lee†, and Peter Luffi
Department of Earth Science, MS-126, Rice University, 6100 Main Street, Houston, Texas 77005, USA

ABSTRACT

Retrograde eclogites (ranging from unaltered eclogite to retrograde blueschist and greenschist mantling the eclogite boulders) from Ring Mountain on the Tiburon Peninsula, near San Francisco, California, were examined for whole-rock major and trace elements to assess protolith compositions and the geochemical signature of fluids associated with retrogression. High field strength elements are highly correlated, indicating relatively immobile and conservative behavior during retrogression. These immobile elements were used to assess the relative losses or gains of other elements during retrogression. Rare earth elements and FeO content show only minimal open-system behavior. The rare earth abundance patterns, FeO contents, and Nb/Ta and Nb/La ratios show that the protoliths of these rocks were most likely normal to enriched mid-oceanic ridge basalts. Mass-balance considerations reveal two independent styles of metasomatic enrichment during retrogression. One style involves coupled enrichment in large ion lithophile elements (Cs, Rb, Ba, K, and Tl), likely caused by fluids from sediments or reaction with sediments. Another style involves coupled enrichment in Cr, Mg, Ni, and Pb, which may reflect overprinting by reaction of eclogite boulders with serpentinite, the latter of which are highly enriched in these elements. Pb is shown here and elsewhere to be nearly universally enriched in serpentinites and is likely to be selectively mobilized into eclogite-serpentinite reaction zones. Because all retrograde lithologies show reaction with serpentinites and sediments, exhumation of the eclogite must have been accompanied by chemical interaction with serpentinites along the entire retrograde path. The simplest interpretation is that the eclogites were transported within a deeply rooted serpentinite channel, presumably formed along the slab-mantle interface by infiltration of slab-derived fluids into the overlying mantle wedge. Physical models of channel flow show that the rapid exhumation rates required to preserve eclogites in a hydrous carrier matrix, such as serpentinite, are possible due to the buoyant and low-viscosity nature of serpentinite. However, the most rapid ascent rates occur during oblique subduction, suggesting that eclogite exhumation could be favored by, but not confined to, oblique subduction zones.

INTRODUCTION

Subduction zones are places where crust is returned and recycled back into the mantle, but the presence of high-pressure metamorphic rocks, such as eclogites, in accretionary prisms indicates that deep crustal materials are, on occasion, exhumed to the surface in convergent margins (Platt, 1993). Geochronologic studies comparing ages of peak metamorphism and exhumation in different accretionary complexes indicate that the time between peak metamorphism (e.g., eclogite formation) and exhumation is <10–20 Ma, corresponding to minimum ascent rates of 2–5 km/Ma (Anczkiewicz et al., 2004; Baldwin et al., 2004; Cloos, 1985). Such rapid exhumation is required in order to avoid complete retrogression of high-grade metamorphic rocks during ascent. Such rapid return is remarkable given that the high densities of eclogites make them neutrally buoyant with respect to most lithologies in the subducted crust and the upper mantle.

The purpose of this paper is to use geochemistry to explore how eclogites return to the surface in ocean-continent subduction. In one class of models, slivers of eclogitized oceanic crust are ripped off during subduction and then transported to the surface by coupled erosion, extension, and return flow in the accretionary prism (Platt, 1986; Schemmann et al., 2008). Another class of models involves transport of eclogite fragments by diapirs or channels associated with low density and hence buoyant matrices, such as sediments (siliciclastics or carbonates) or serpentinites (Ernst, 1970; Ernst et al., 1997; Guillot et al., 2001; Moore, 1984; Schwartz et al., 2001). One of the difficulties in testing these hypotheses is that eclogite boulders often occur in highly tectonized and jumbled terranes, e.g., mélanges, so their original high-pressure structural relationships with surrounding rocks are poorly preserved. Here we investigate the geochemical signatures of variably retrograde eclogite lenses found in the Franciscan mélange, which is part of a Jurassic–Cretaceous accretionary complex that extends from California's central coast to coastal northern California (Platt, 1975). The purpose of examining variably retrograde eclogite lenses is to determine how the chemistry of eclogites changes during retrogression, providing insight into exhumation processes. We conducted a case study of Franciscan eclogites from the Tiburon Peninsula, just north of San Francisco, California. We show that the trace element geochemistry of the retrograde eclogites is consistent with transport from depth within a serpentinite matrix. We then use these observations to speculate on the nature of eclogite exhumation in ocean-continent subduction zones.

Case Study of Retrograde Franciscan Eclogites from the Tiburon Peninsula, California

The Franciscan mélange, associated with the accretionary wedge formed during Farallon plate subduction beneath North America, consists largely of graywacke, chert, and basaltic

*Present address: Department of Geological Sciences, Brown University, 324 Brook Street, Box 1846, Providence, Rhode Island 02912, USA.
†Corresponding author: ctlee@rice.edu.

Geosphere; October 2009; v. 5; no. 5; p. 426–438; doi: 10.1130/GES00502.1; 10 figures; 1 table.

volcanic units disrupted by tectonic blocks and slivers of low-grade metamorphic rocks, such as greenschists and serpentinites, and medium- to high-grade metamorphic rocks, such as blueschists, amphibolites, and eclogites. Peak metamorphic ages for the high-grade rocks in the Franciscan mélange are between 149 and 169 Ma, based on Lu-Hf ages of eclogites and amphibolites (Anczkiewicz et al., 2004).

We collected samples from Ring Mountain, located on the Tiburon Peninsula in California (Catlos and Sorensen, 2003; Tsujimori et al., 2006a). Most of this region is made up of serpentinite and greenschist, within which are occasional large boulders and lenses of eclogite. We examined 11 samples, representing different parts of an eclogite boulder, in order to investigate protolith compositions and the effects of retrograde metasomatism on composition. We categorized these samples into three lithologies (Fig. 1), following descriptions given in previous studies (Saha et al., 2005; Tsujimori et al., 2006a). First are the eclogite cores of the high-grade lenses (Fig. 1A). These eclogites consist of ~40% garnet, ~60% omphacite pyroxene, and small amounts of chlorite alteration rims to pyroxenes (accessory phases include rutile and epidote). Eclogites overprinted by blueschists make up the second category and represent the first retrograde envelope surrounding the eclogite core (Fig. 1B). The blueschist-overprinted eclogites consist of <50% garnet, >30% chlorite, >50% glaucophane, and ~10% phengite; accessory minerals include titanite, apatite, Fe-oxides, and quartz. Garnets commonly show chlorite breakdown rims and all pyroxenes appear to have been converted to glaucophane or chlorite. The third category is made up of chloritized eclogite, representing the outermost retrograde rind (Fig. 1C). Pyroxene has been mostly transformed into glaucophane or chlorite with chlorite mode exceeding glaucophane due to replacement of glaucophane by chlorite. The mineralogy consists of <40% garnet, 40% chlorite, <20% glaucophane, and <1% phengite.

Based on detailed thermobarometric studies of relict prograde and retrograde mineralogies, Tsujimori et al. (2006a) showed that these eclogites followed a counterclockwise pressure-temperature (*P-T*) path and were exhumed along decreasing thermal gradients, perhaps due to progressive refrigeration of the mantle wedge by the subducting Farallon plate. The eclogites underwent peak metamorphism at ~2.2 GPa (70 km), while their blueschist retrogression occurred at ~1.1 GPa (35 km). Based on Lu-Hf for peak metamorphism and Ar-Ar ages of 147 Ma for blueschist retrogression (Anczkiewicz et al., 2004; Tsujimori et al., 2006a), Tsujimori (2006a) suggested that exhumation rates might have been as fast as ~5 km/Ma, similar to that inferred for exhumation rates in ultrahigh-pressure metamorphic terranes.

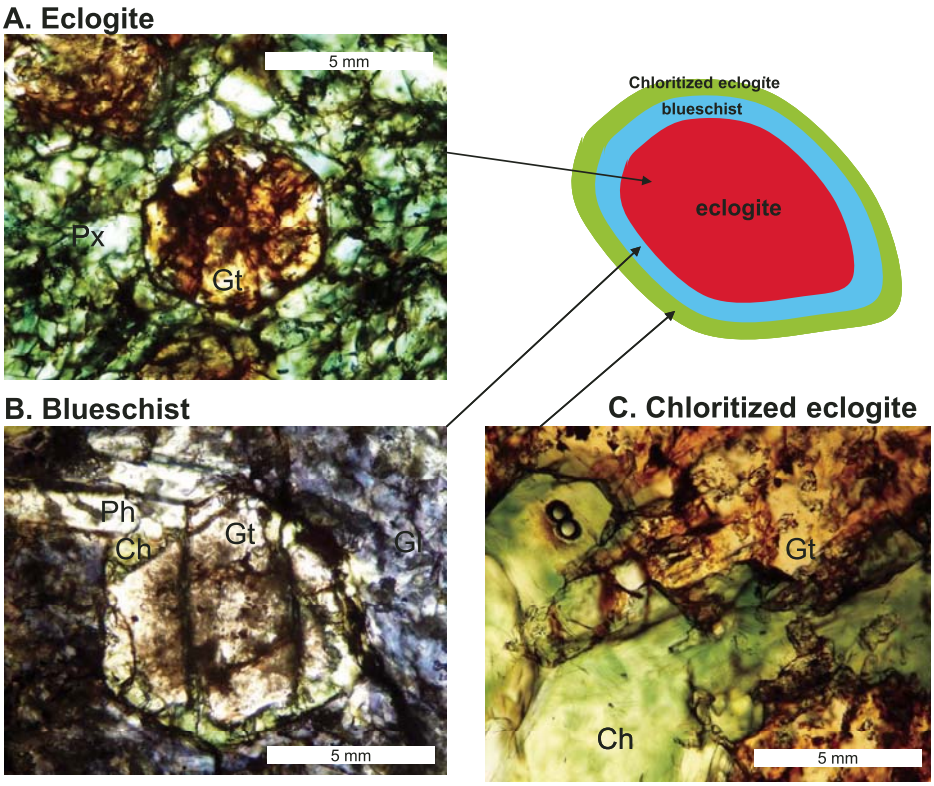

Figure 1. Photomicrographs of representative metamorphic rocks and their spatial relationships within eclogite boulders. (A) Eclogite core with fresh garnet (Gt) and omphacitic pyroxene (Px). (B) Blueschist mantle, representing the first retrograde rim around the eclogite core. Note glaucophane (Gl) matrix, muscovite (Mu), and breakdown of garnet rims to chlorite (Ch). (C) Chloritized eclogite representing the outermost retrograde mantle of the eclogite boulder. Note extensive chloritization and preservation of relict garnets.

Previous Geochemical Studies on the Tiburon Eclogites

Trace element and isotopic studies of the Tiburon eclogites were conducted by Saha et al. (2005), who argued that the Tiburon eclogites and associated mafic metamorphic rocks had an island arc basalt protolith, based on slightly low Nd isotopic compositions, high Pb isotopic compositions, and in particular low Ce/Pb ratios. Low Ce/Pb ratios in basalts are generally thought to indicate preferential mobilization of Pb, presumably due to hydrous melting, and therefore are a signature of arc basalts. However, Pb is highly mobile during metamorphic reactions involving fluids, begging the question of whether the Pb contents (and Pb isotopic composition) of the eclogites truly reflect the protolith composition. In part, the goal of this study is to assess the role of open-system behavior during retrograde metamorphism on the geochemistry of the eclogites.

METHODS

Samples were crushed and powdered in a Spex mill. One aliquot was sent to Washington State University, Pullman, for major element and select trace element analyses by X-ray fluorescence (XRF). Another aliquot (50 mg of powder) was dissolved for major and trace element analysis by solution inductively coupled plasma–mass spectrometry (ICP-MS) at Rice University, Houston. Samples were dissolved using 0.25 mL of a 1:1 mixture of concentrated HF and $HClO_3$, heated at 140 °C, and followed by complete dry down at 170 °C. This procedure was repeated and the final dry down was taken up in 125 mL of 2 wt% HNO_3 (one drop of 6 N HCl was added to keep Fe in solution). Procedural blanks and external standards (U.S. Geological Survey standards BHVO1 and BIR1) were processed through the same procedure

simultaneously. A known quantity of indium was added to each solution to serve as an internal standard for instrumental drift during analysis. Solutions were introduced into a Thermo-Finnigan Element 2 ICP-MS by free-aspiration via an Elemental Scientific Teflon nebulizer (100 μL/min uptake) attached to a cyclonic spray chamber. Measurements were done in low and medium mass resolution modes, the former for trace elements and the latter for major elements and those trace elements in the mass range of 45–66 amu, where isobaric molecular interferences occur and can be resolved in medium mass resolution. Signal intensities were corrected for instrumental drift by monitoring In, and then converted to concentrations by calibration against BHVO1 and BIR1 basalt standards (using standard values from the Max Planck Institute GeoReM database; http://georem.mpch-mainz.gwdg.de/).

RESULTS

Geochemical data for the core to rim series (e.g., eclogite core to blueschist and greenschist mantles) are shown in Table 1 (data have not been normalized to 100%). Major element contents of the eclogite cores are broadly similar to basalts with the exception of the high Na contents, presumably reflecting a seawater-altered oceanic crust protolith (Fig. 2). Retrogression from eclogite to blueschist to greenschist is associated with decreasing SiO_2 and Na_2O but increasing Al_2O_3 content (Figs. 2B, 2D). MgO and K_2O rise in the blueschists and then decrease in the greenschist. The high K_2O contents are correlated with the appearance of phengite in the blueschists. Additional geochemical transitions as a function of Na content are shown in Figure 3. Figure 3A shows how Mg is enriched in the blueschists. Figure 3B shows that the retrograde lithologies, with the exception of one sample, are elevated in Cr relative to the eclogite core. Figure 3C shows higher Ni contents in blueschists, but similar Ni contents in greenschist and eclogite. Figure 3D shows that Li is strongly correlated with Na, indicating that retrogression of eclogite is accompanied by Li depletion.

To more meaningfully display all the geochemical data, however, relative enrichments or depletions were calculated by assuming that the high field strength elements (HFSEs; Ti, Zr, Nb, Ta) were immobile. This is a common assumption in metamorphic petrology as well as in soil geochemistry because such elements are much less soluble in aqueous fluids than monovalent or divalent cations (Ague, 2003; Ague and van Haren, 1996; Brimhall and Dietrich, 1987; Little and Lee, 2006; van der Straaten et al., 2008). Although perfect immobility is probably never attained, the high degree of correlation between Nb, Ti, and Ta (Fig. 4) suggests that the immobile approximation of these elements is probably reasonable for this case study (as the likelihood of each being equally mobile is small). We note that correlations of Zr with the elements shown in Figure 4 are poor, and hence they are not shown. This may be due partly to the fact that Zr measurements were done by XRF, whereas Ti, Nb, and Ta were done by solution ICP-MS, and therefore the latter set represent internally consistent data (Zr was not measured by solution ICP-MS due to our inability to dissolve all zircons). In any case, Nb/Ta and Nb/Ti ratios are similar to mid-oceanic ridge basalt (MORB) and ocean island basalts, a feature to which we will return.

Taking Nb, Ta, and Ti as immobile, mass loss or gain during retrogression relative to the original protolith mass, M_{rock}/M_o, can be estimated with the following equation (Brimhall and Dietrich, 1987):

$$\frac{M_{rock}}{M_o} = \frac{C_o^i}{C_{rock}^i}, \quad (1)$$

where M_{rock} is the mass of the retrograde lithology, M_o is the original mass of the protolith, C_{rock}^i is the concentration of an immobile element in the retrograde lithology, and C_o^i is the concentration of the same immobile element in the protolith. Thus, for an immobile element, an increase in its concentration requires mass loss from the system during retrogression. Conversely, a decrease in its concentration indicates mass gain. These mass conservation principles can be extended to all other elements to assess their mobility (relative to the immobile element *i*). The percentage increase or decrease in mass of a given element, $\frac{\Delta m_{rock}^j}{m_o^j}$, during retrogression is given by (Brimhall and Dietrich, 1987; Little and Lee, 2006):

$$\frac{\Delta m_{rock}^j}{m_o^j} = \frac{\left(C_o^i / C_{rock}^i\right) C_{rock}^j - C_o^j}{C_o^j} \times 100, \quad (2)$$

where C_{rock}^j is the concentration of mobile element *j* in the retrograde lithology, C_o^j is the concentration of mobile element *j* in the protolith, m_o^j is the mass of mobile element *j* in a given amount of protolith, and ΔC_o^j is the change in mass of element *j* during retrogression.

For our case study, we assume the eclogite core represents the protolith and we adopt Ti as our immobile element *i*. Unfortunately, however, the Ti contents in our two eclogite core samples (UH1 and UH8) differ considerably (Fig. 4A). The Ti and Nb contents of UH8 are the only elemental concentrations that differ substantially between UH1 and UH8. In TiO_2 versus Na_2O plots (not shown), UH8 appears to be an outlier, so we attribute the low Ti contents of UH8 to nugget effects associated with dissolution of heterogeneous samples wherein Ti is housed primarily in accessory oxide phases. We thus take the Ti content of UH1 as an estimate of the protolith's Ti content. Figure 5 shows percent mass loss or gain of individual elements relative to the average of the two eclogite samples (by definition, Ti mass change is zero). The red horizontal bar qualitatively defines the regions of 30% mass loss or gain for reference. We note that the HFSEs all plot close to zero (Fig. 6), suggesting that our choice of Ti protolith concentration is reasonable. If UH8's Ti value was used instead, all the HFSEs would have been shifted considerably from the zero line, inconsistent with their presumed immobile behavior.

The most obvious features in Figure 5 are as follows. K, Cs, Rb, Ba, Tl, and Cu show the most pronounced enrichments (>300%), particularly in the blueschists. Figures 6A and 6B show that the enrichments in Ba, Rb, and K (as well as Cs and Tl; not shown) are correlated. Sr also shows substantial enrichments, but the most pronounced enrichments are in the greenschists, and hence Sr enrichments are decoupled from Ba, Rb, and K. Li and Na show depletions (Fig. 5) and therefore are anticorrelated to enrichments in Ba, Rb, K, Cs, and Tl. Cr shows relative enrichments of 200%–800% (Figs. 5 and 6C–6F), but such enrichments show no correlation with enrichments in large ion lithophile elements (LILEs) like Ba (Fig. 6C). Cr enrichment instead appears to be correlated with smaller enrichments in Mg and Ni (Figs. 6D, 6E); this correlation holds even if the most Cr- and Mg-enriched sample is ignored. The covariation diagrams in Figure 6 have additional significance in that any correlations are essentially independent from choice of normalizing element (e.g., the immobile element of choice). We note that choosing a different immobile element could cause those elements that show moderate (<50%) enrichment or depletion factors, such as Mg and Ni, to shift about the zero line. However, the fact that the large Cr mass changes correlate with the smaller Mg and Ni mass changes (Fig. 6) suggests that Mg and Ni have undergone relative enrichments. What is surprising is that Cr enrichment is strongly correlated with Pb enrichment, even though these two elements in general do not behave geochemically similarly.

Rare earth element (REE) mobility in Figure 5 appears to be largely limited as nearly all samples cluster around zero for the heavy

TABLE 1. MAJOR AND TRACE ELEMENT COMPOSITIONS

	Eclogite			Chloritized eclogite								
	UH1		UH8	UH3			UH6		UH11		UH12	
	ICP (wt%)	XRF (wt%)	ICP (wt%)	ICP (wt%)	rsd (n = 2)	XRF (wt. %)	ICP (wt%)	XRF (wt%)	ICP (wt%)	XRF (wt%)	ICP (wt%)	XRF (wt%)
SiO_2		50.67	53.48			41.91		42.91		44.57		43.88
TiO_2	2.219	2.52	1.180	1.304	0.058	1.73	1.408	1.73	1.96	2.28	1.308	1.60
Al_2O_3	10.46	11.02	10.73	17.07	0.017	18.60	16.78	18.82	14.82	16.12	15.25	18.09
FeO*	10.27	11.05	10.79	11.7	0.015	12.67	10.44	11.41	10.42	11.36	9.81	11.10
MnO	0.2049	0.23	0.2031	0.309	0.004	0.33	0.242	0.26	0.153	0.17	0.166	0.19
MgO	7.82	7.40	7.03	6.734	0.021	6.31	6.27	6.15	9.32	8.94	6.986	6.93
CaO	11.0	11.90	10.97	14.94	0.017	16.23	15.69	17.01	12.96	13.97	15.02	16.27
Na_2O	4.87	5.03	4.48	1.156	0.006	1.22	1.014	1.11	1.864	1.99	1.384	1.54
K_2O	0.0667	0.10	0.0910	0.169	0.009	0.19	0.144	0.18	0.313	0.34	0.184	0.21
P_2O_5	0.0836	0.09	0.0958	0.797	0.014	0.81	0.423	0.44	0.236	0.26	0.167	0.19
Sum		100				100		100		100		100
LOI %		0.96				1.85		1.40		2.00		1.05
(ppm)												
Li	38.4		37.4	7.05	0.019		4.69		8.70		4.84	
Be	1.2		1.19	0.67	0.004		0.65		1.34		0.92	
Sc	42.3	45.1	44.2	44.9	0.003	50.2	42.9	48.8	43.0	47.7	41.3	49.9
V	405	444	409	325	0.009	356	342	377	358	387	339	399
Cr	102	117	94.7	284	0.031	268	249	270	273	305	254	283
Co	30.9		31.9	27.4	0.022		22.5		53.4		29.4	
Ni	74.2	90.1	62.4	75.5	0.023	90	75.1	90	107	126	79.0	102
Cu	6.50	11.5	7.3	27.9	0.011	33	23.7	27.5	48.8	54.7	24.2	30.1
Zn	110	120	143	94.3	0.023	96.1	87.0	90.5	134	145	111	120
Ga	12.6	12.5	13.4	21.3	0.002	24	24.1	23.1	19.7	21	21.6	24.8
Rb	3.59	3.8	3.77	5.50	0.021	4.7	4.93	5.8	6.03	7	2.79	2.4
Sr	35.4	36.7	29.8	447	0.005	459	505	506	456	475	527	542
Y	52.1	54.2	47.1	39.6	0.030	44	41.5	43	43.8	48	43.4	48
Zr		177				100		94		98		98
Nb	8.95	9.1	5.0	5.62	0.051	6.1	6.0	5.1	8.3	8.7	5.5	4.5
Cs	0.07		0.089	0.121	0.032		0.122		0.069		0.073	
Ba	71.4	70.1	83.4	73.0	0.014	64	87.3	82	115	116	50.0	46
La	8.28	9	6.35	5.17	0.028	10	5.72	9	6.45	11	6.01	11
Ce	22.9	25	17.1	13.1	0.037	17	14.5	19	16.8	20	15.5	22
Pr	3.69		2.85	2.07	0.018		2.32		2.67		2.44	
Nd	18.6	21.1	14.7	10.7	0.017	13	11.9	14	14.0	15	12.5	15
Sm	5.32		4.34	3.46	0.008		3.97		4.71		4.19	
Eu	1.55		1.33	1.29	0.009		1.47		1.79		1.51	
Gd	6.26		5.39	4.70	0.019		5.42		6.33		4.38	
Tb	1.08		0.962	0.846	0.019		0.967		1.131		0.762	
Dy	7.44		6.65	5.68	0.016		6.41		7.26		5.33	
Ho	1.75		1.55	1.31	0.006		1.40		1.51		1.52	
Er	5.19		4.62	4.15	0.006		4.21		4.15		4.47	
Tm	0.77		0.68	0.66	0.003		0.63		0.56		0.66	
Yb	4.34		3.79	3.82	0.012		3.62		3.13		3.72	
Lu	0.64		0.572	0.563	0.009		0.522		0.431		0.529	
Ta	0.54		0.324	0.335	0.047		0.364		0.513		0.364	
Tl	0.03		0.028	0.029	0.027		0.024		0.055		0.025	
Pb	5.38		1.4	13.6	0.010		15.5		14.6		15.0	
Th	0.56		0.417	0.395	0.021		0.428		0.521		0.434	
U	0.56		0.457	0.908	0.017		0.904		0.560		0.321	
Cr/Nb	11.4		19.0	50.6			41.5	53.0	32.7	35.0	46.4	62.8
Ni/Nb	8.29		12.48	13.44			12.50	17.69	12.79	14.49	14.41	22.56
Ce/Pb	4.26		12.27	0.96			0.94		1.15		1.03	
Nb/La	1.08		0.79	1.09			1.05		1.29		0.91	
Nb/Ta	16.5		15.4	16.8			16.5		16.3		15.1	
Mg#	0.58	0.54	0.54	0.51		0.47	0.52	0.49	0.61	0.58	0.56	0.53

(*continued*)

TABLE 1. MAJOR AND TRACE ELEMENT COMPOSITIONS (*continued*)

	Blueschist											
	UH2		UH5		UH7		UH9			UH10		
	ICP (wt%)	XRF (wt%)	ICP (wt%)	XRF (wt%)	ICP (wt%)	XRF (wt%)	ICP (wt%)	rsd (n = 2)	XRF (wt%)	ICP (wt%)	XRF (wt%)	
SiO_2		49.96		46.08		48.50			49.77		43.18	
TiO_2	2.862	3.35	2.7	3.20	1.986	2.36	2.23	0.018	2.65	0.746	1.09	
Al_2O_3	14.16	14.85	15.03	16.51	15.63	16.87	13.86	0.012	14.98	10.77	12.29	
FeO*	12.55	13.49	13.96	15.57	8.28	8.91	12.44	0.004	13.27	9.44	10.51	
MnO	0.233	0.26	0.37	0.40	0.162	0.18	0.217	0.008	0.23	0.173	0.18	
MgO	10.27	9.79	8.011	7.91	7.736	7.41	9.779	0.011	9.25	10.37	10.19	
CaO	1.614	1.79	4.841	5.35	9.423	10.37	3.761	0.005	4.05	15.36	16.26	
Na_2O	4.053	4.33	2.734	3.00	2.587	2.77	3.675	0.005	3.93	2.007	2.21	
K_2O	1.814	1.82	1.632	1.66	2.6	2.49	1.741	0.012	1.72	0.264	0.30	
P_2O_5	0.333	0.36	0.287	0.31	0.134	0.15	0.129	0.005	0.14	4.142	3.80	
Sum		100		100		100			100		100	
LOI %		3.63		3.48		2.57			3.36		1.15	
(ppm)												
Li	26.8		22.9		18.4		25.7	0.000		6.90		
Be	1.5		1.17		1.50		0.67	0.008		1.40		
Sc	45	57.5	48.8	62.6	41.5	47.7	38.2	0.013	52.7	35.8	40.9	
V	402	436	403	433	356	388	264	0.009	297	275	314	
Cr	135	140	42.1	48.6	283	273	369	0.003	332	296	287	
Co	30		32.2		26.1		63.2	0.010		39.3		
Ni	128	143	57	66	77.5	87	116	0.001	130	114	134	
Cu	35.6	37.6	67.9	68.5	39.6	39.5	27.2	0.005	33	17.6	22.4	
Zn	164	173	130	136	107	116	180	0.000	190	154	167	
Ga	16.0	17.6	18.6	18.2	19.4	22.4	14.4	0.001	15.5	15.7	15	
Rb	50.5	50.7	44.9	45	67.3	64.3	43.86	0.006	43.5	5.31	5.1	
Sr	30.5	31.9	103	107	264	274	85.5	0.010	87.7	357	358	
Y	26.2	27.7	55.7	59	44.1	45	33.1	0.004	35	58.9	61	
Zr		177		197		117			175		116	
Nb	12.5	13.4	12.2	12.2	9.3	9.7	7.157	0.009	6.9	2.7	4.1	
Cs	0.46		0.383		0.423		0.578	0.008		0.126		
Ba	1185	1217	1144	1170	1199	1170	1291	0.006	1294	72.9	70	
La	8.26	10	9.41	14	6.14	5	8.54	0.009	9	15.08	9	
Ce	18.8	18	24.3	28	15.4	18	24.7	0.002	32	35.0	35	
Pr	2.84		3.73		2.44		3.88	0.000		5.51		
Nd	14.1	15	19.3	20	12.7	16	20.2	0.000	21	27.5	26	
Sm	4.19		6.16		4.18		5.64	0.002		8.26		
Eu	1.12		1.99		1.56		1.50	0.022		2.66		
Gd	4.84		7.88		5.95		6.03	0.019		9.69		
Tb	0.77		1.38		1.09		0.923	0.025		1.614		
Dy	4.48		8.76		7.09		5.55	0.021		9.72		
Ho	0.94		1.88		1.47		1.21	0.007		2.10		
Er	2.79		5.78		4.08		3.64	0.008		5.75		
Tm	0.43		0.89		0.57		0.55	0.011		0.80		
Yb	2.67		5.27		3.13		3.38	0.008		4.70		
Lu	0.40		0.782		0.437		0.494	0.006		0.664		
Ta	0.76		0.798		0.537		0.411	0.002		0.235		
Tl	0.41		0.403		0.490		0.395	0.001		0.048		
Pb	10.2		9.1		9.2		27.8	0.004		12.6		
Th	1.08		1.118		0.483		0.479	0.014		1.447		
U	0.53		0.437		0.687		0.741	0.003		1.018		
Cr/Nb	10.8	10.5	3.4	4.0	30.5	28.2	51.5		48.1	108.8	70.1	
Ni/Nb	10.28	10.66	4.66	5.39	8.34	9.01	16.17		18.78	41.95	32.61	
Ce/Pb	1.84		2.68		1.67		0.89			2.77		
Nb/La	1.51		1.30		1.51		0.84			0.18		
Nb/Ta	16.4		15.3		17.3		17.4			11.6		
Mg#	0.59	0.56	0.51	0.48	0.62	0.60	0.58		0.55	0.66	0.63	

Note: For ICP-MS (inductively coupled plasma–mass spectrometry) measurements, all major elements and Ni, Cu, Zn, V, Sc, Ti, P, and Cr were done in medium mass resolution; all other elements were done in low mass resolution. XRF—X-ray fluorescence; rsd—relative standard deviation; LOI—loss on ignition.

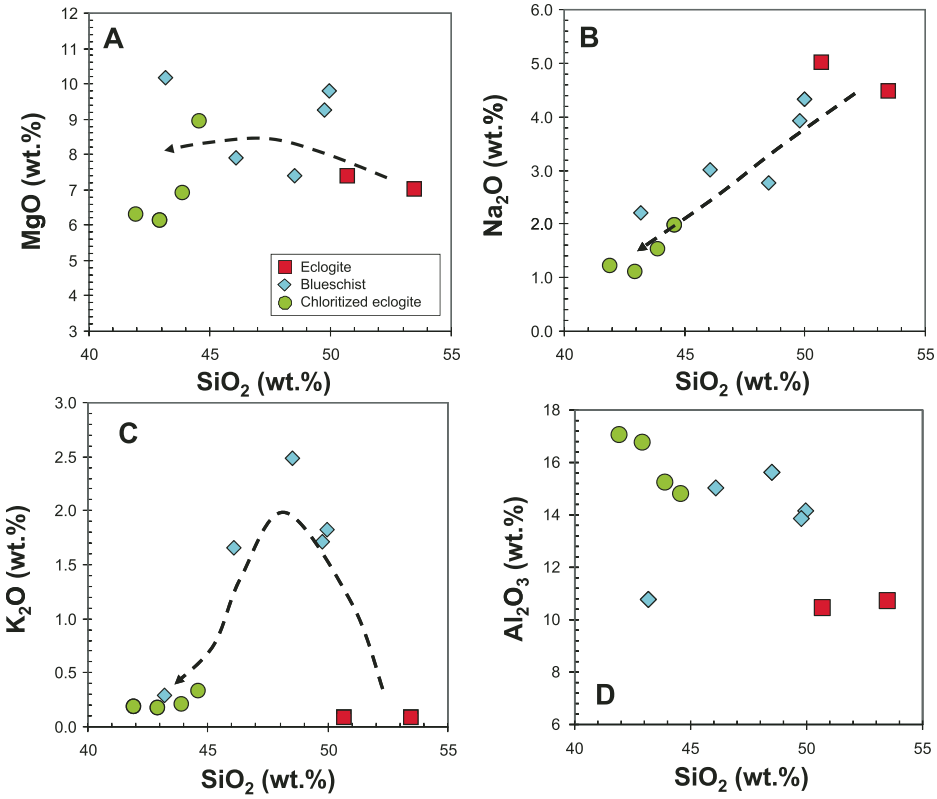

Figure 2. Compositions of metamorphic rocks. (A) MgO versus SiO_2 (in wt%). (B) Na_2O versus SiO_2. (C) K_2O versus SiO_2. (D) Al_2O_3 versus SiO_2. Dashed arrowed curves represent schematic direction of retrograde metamorphism. Symbols are shown in the legend.

REEs. One blueschist sample (UH10) appears to show substantial relative REE enrichment, but this is certainly due to its anomalously low Ti content, because the absolute REE contents are only slightly higher than the other blueschists. In any case, the REE systematics in the form of primitive mantle normalized values (Fig. 7A) show that all of the lithologies in this study have REE patterns similar to those of MORBs, albeit with slight enrichments in the light REEs. These slight enrichments in the light REEs are most pronounced in the retrograde lithologies, suggesting that there has been some infiltration of light REE components.

Ce/Pb is often used as a provenance indicator in basaltic magmas because Ce and Pb are thought to have identical geochemical behaviors during anhydrous mantle melting (Hofmann et al., 1986). During hydrous melting, however, it is thought that Pb is more mobile, resulting in fractionation of Ce/Pb ratios and generating the low Ce/Pb ratios characteristic of arc basalts. Figure 8 shows that decreasing Ce/Pb ratio is associated with increasing Pb contents with little to no changes in Ce content. The lowest Ce/Pb ratios are associated with the blueschists, consistent with the Pb enrichment inferred from simple mass-balance approaches. In all likelihood, even the eclogites have also undergone considerable Pb enrichment.

DISCUSSION

Geochemical Constraints on Protolith

As shown in the Results section and in Figures 4 and 5, the HFSEs (Nb, Ta, Zr, Ti) and the REEs seem to have undergone less disturbance during retrogression. This is evidenced by the constant Nb/Ta and Nb/Ti ratios and the clustering of REE mass changes around zero in Figure 5 for the entire suite of lithologies. The low mobility of these elements allows us to use their relative proportions as geochemical fingerprints of possible protoliths. For example, Nb/La and Nb/Ta ratios cluster around 1 and 17, respectively. These values coincide with values of the model bulk silicate Earth (e.g., the Earth's primitive mantle; McDonough and Sun, 1995), MORBs, and ocean island basalts (hotspot magmas), but contrast strongly with the low Nb/La and Nb/Ta ratios seen in island arc basalts (Figs. 4B and 7B) (Hofmann, 1988; Hofmann, 1997; Kelemen et al., 1990). The absolute abundances of the heavy REEs are also very similar to those of MORBs, unlike arcs, which have slightly lower heavy REE abundances, as can be seen in Figure 7A (Sun and McDonough, 1989). The REEs normalized to model bulk silicate Earth (McDonough and Sun, 1995), and plotted in order of increasing atomic weight (and increasing compatibility in the solid), exhibit flat to slightly negatively sloped abundance patterns. Such patterns are typical of enriched MORBs (e.g., seamounts) or ocean island basalts (Fig. 3D) (Hofmann, 1997; Kelemen et al., 2003; Sun and McDonough, 1989), but not island arcs.

The FeO contents (all Fe taken as Fe^{2+}) of the eclogites are ~10 wt%, which is higher than that seen in island arc basalts (~8 wt%) and on the high end of MORBs. High Fe contents could be related to high-temperature and high-pressure melting of the mantle if the eclogite protolith was once a basaltic liquid. Assuming that the eclogite protoliths represent fractionated basalts, we can estimate the primary parental magma of the protolith by correcting for crystal fractionation (assumed to be dominated by olivine) until the hypothetical magma is in equilibrium with a mantle source typical of the upper mantle [molar Mg/(Mg + Fe) ~0.89–0.9; Fig. 9]. Mg-Fe exchange between olivine and liquid can then be used to estimate temperature (Courtier et al., 2007; Putirka et al., 2007; Roeder and Emslie, 1970), yielding temperatures of ~1500 °C (Fig. 9). These temperatures, however, are likely to be upper bounds because the addition of Fe-rich cumulate crystals during igneous differentiation, Fe addition during hydrothermal alteration, and preferential mass loss during metamorphism could result in an elevation of Fe content. We thus conclude that our calculated temperatures are similar to oceanic plateaus, hotspots, seamounts (>1400 °C), and MORBs (1300–1400 °C) (Courtier et al., 2007; Herzberg et al., 2007; Putirka et al., 2007).

Based on the above trace element and major element compositions, we estimate that the protoliths of the Ring Mountain eclogites were MORBs or enriched MORBs and thus represent oceanic crust or seamounts. Previous studies argued that the protoliths were island arc basalts on the basis of Pb isotopic compositions and low Ce/Pb ratios (Saha et al., 2005), but as we discussed above, low Ce/Pb ratios are a feature of preferential Pb addition during retrogression.

Geochemical Signatures of Retrogression and the Role of Serpentinites

There appear to be at least two types of metasomatic enrichments associated with retrogression. As outlined in the Results section, one type of enrichment is characterized

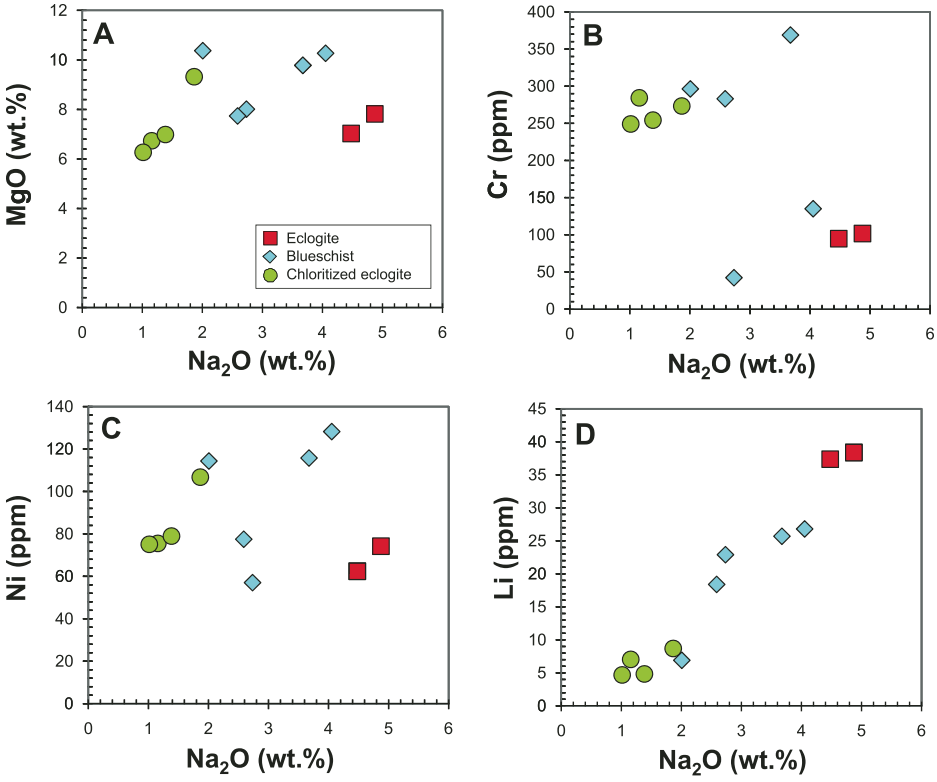

Figure 3. Compositions of metamorphic rocks. (A) MgO versus Na_2O (in wt%). (B) Cr in ppm (by weight) versus Na_2O (wt%). (C) Ni (ppm) versus Na_2O (wt%). (D) Li (ppm) versus Na_2O (wt%). Symbols are denoted in the legend.

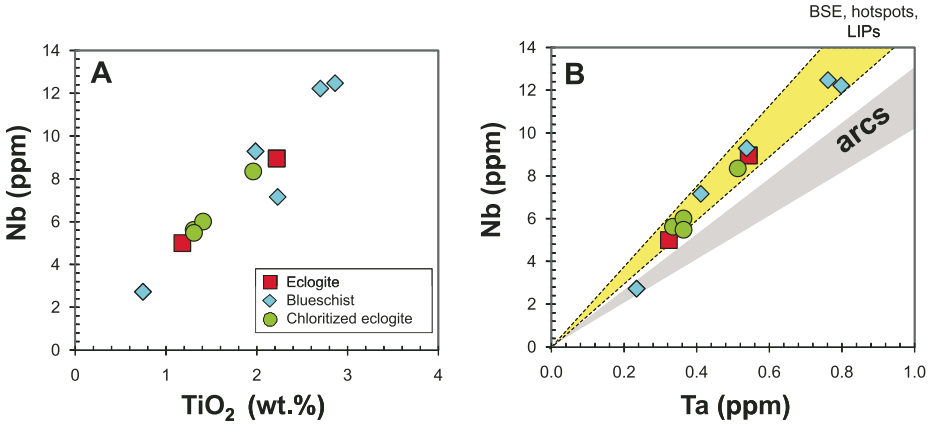

Figure 4. (A) Nb (ppm by weight) versus TiO_2 (wt%). (B) Nb versus Ta (ppm by weight). Gray shaded region represents range of Nb/Ta ratios for island arc basalts. Yellow shaded (outlined with dashed line) region represents range of Nb/Ta ratios for mid-ocean ridge basalts, ocean island basalts, and bulk-silicate Earth.

by the addition of LILEs such as K, Rb, Cs, Ba, and Tl. Similar metasomatic enrichments are found in eclogites and blueschists from Catalina Island, California, and were used to argue that these mafic metamorphic rocks were "bathed" in LILE-enriched fluids, since these elements are thought to be fluid mobile (Catlos and Sorensen, 2003; Giaramita and Sorensen, 1994; Sorensen and Grossman, 1989). These elements ultimately must derive from fluids released from a source enriched in these elements. Metamorphosed sediments, such as pelites, are probably the most likely source for these elements (Bebout, 2007; Bebout and Barton, 2002; Catlos and Sorensen, 2003). In contrast, Na and Li are rather depleted in the blueschists and greenschists compared to the eclogite protolith. This seems counterintuitive because their geochemical behaviors should be similar to the other LILEs; in addition, Na is a major constituent in glaucophane. However, such depletions have been shown in similarly retrograde eclogites from Tian Shan, China (van der Straaten et al., 2008).

The second metasomatic overprint is characterized by enrichments in Cr, Mg, Ni, and Pb, and appears to be independent of the LILE enrichments. Enrichments in Cr, Mg, and Ni have been seen in retrograde eclogites from Tian Shan, China (van der Straaten et al., 2008). Enrichments in Cr and Mg have also been seen in the envelopes of eclogites and amphibolites in contact with serpentinized ultramafics in the Catalina mélange complex in California (Bebout and Barton, 2002). Van der Straaten et al. (2008) suggested that these enrichments in Cr, Mg, and Ni were due to reaction of the eclogites with a serpentinite matrix during retrogression because these elements are enriched in the ultramafic protoliths of serpentinites.

The origin of Pb is less clear. Pb enrichments could derive from pelitic-sourced fluids, but the correlation of Pb and Cr enrichment (Fig. 6F) suggests that the Pb enrichment is coupled with Cr, Mg, and Ni enrichments. If the latter are associated with serpentinite-derived fluids, the implication is that Pb may also be related to serpentinites. Although we have not studied the serpentinites in Ring Mountain because they are scattered throughout the mélange and may not be directly related to the eclogite boulders, Pb enrichment (and low Ce/Pb) appears to be a universal feature of serpentinized peridotites in ocean basins and arc environments. For example, extremely high Pb anomalies (as much as 40 times that of primitive mantle, which approaches the levels seen in continental crust) have been found in serpentinized ophiolites (Li and Lee, 2006) and abyssal peridotites (Kelemen et al., 2007; Niu, 2004) (Fig. 3A). The origin of high Pb in serpentinites is not known, but Pb is likely introduced from seawater during the serpentinization process because Pb enrichments are much less common in unserpentinized mantle xenoliths (Lee, 2005). It has been suggested that the high Pb content in serpentinites may be a global feature, perhaps even resolving the Pb mass balance for the silicate Earth (Godard et al., 2005; Kelemen et al., 2007). It is thus reasonable to speculate that the Pb enrichment in the retrograde eclogites may have derived from serpentinites

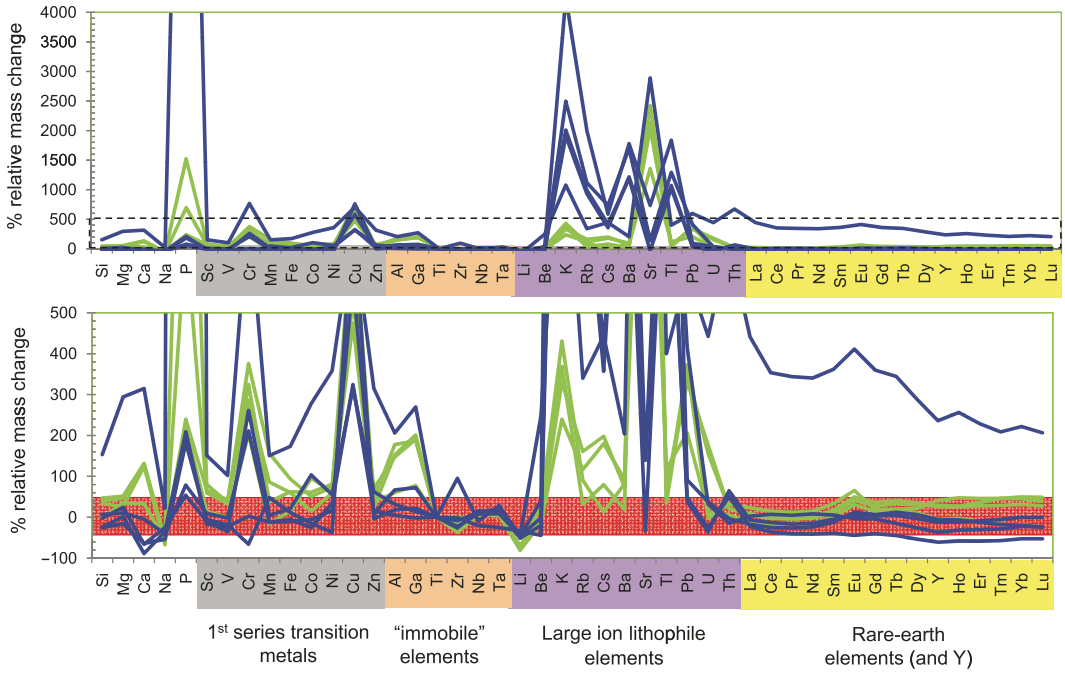

Figure 5. Percent relative mass change for each element relative to an eclogite protolith (UH1) and assuming that Ti is perfectly immobile. Top figure shows all data. Bottom figure is an enlarged view. Zero line represents no mass gain or loss. Red shaded horizontal bar shows ±30% uncertainty for reference.

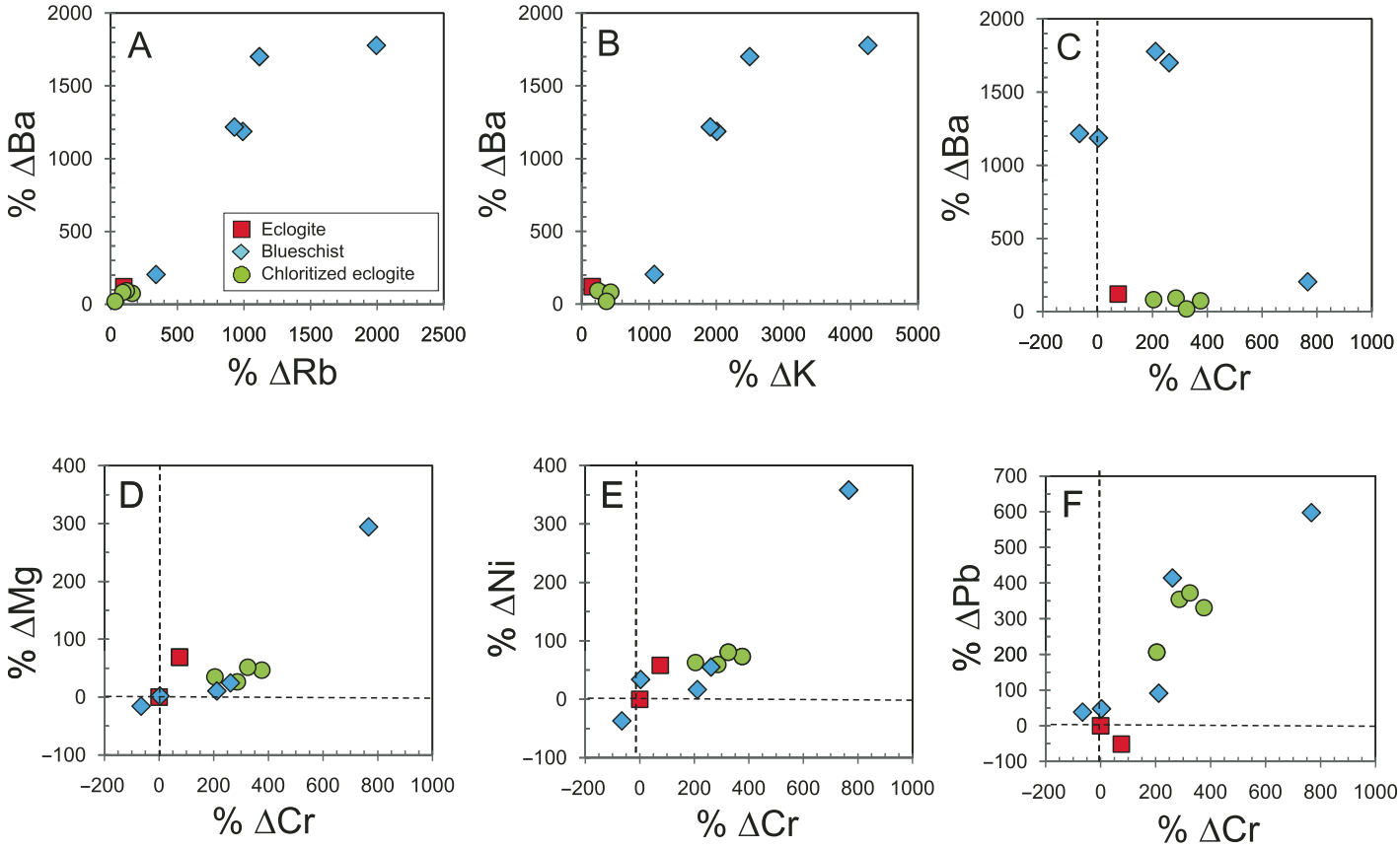

Figure 6. Relative mass changes for select elements in Figure 5 plotted against each other to highlight correlations. (A) Ba versus Rb. (B) Ba versus K. (C) Ba versus Cr. (D) Mg versus Cr. (E) Ni versus Cr. (F) Pb versus Cr. Dashed lines indicate zero lines where mass gain or loss equals zero.

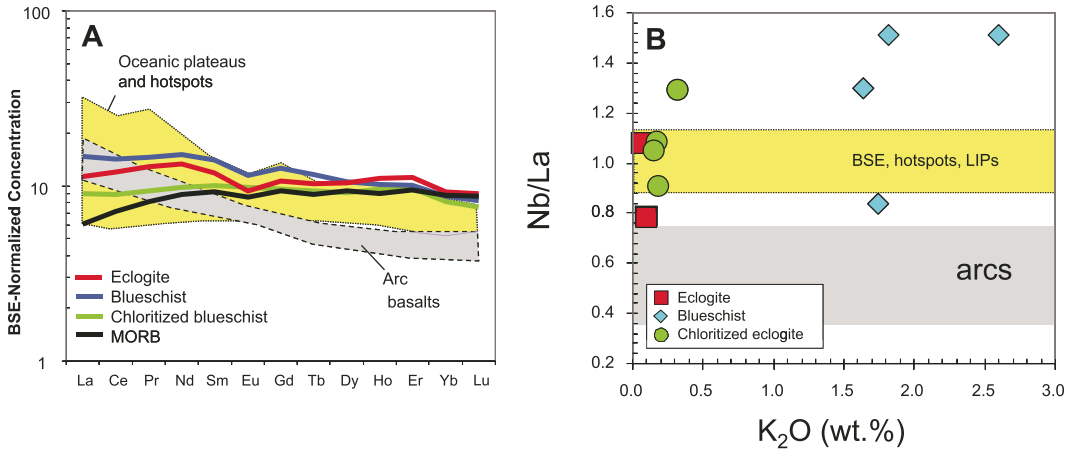

Figure 7. (A) Bulk silicate earth (BSE) normalized concentrations of rare earth elements. Red, blue, and green lines represent average eclogite, blueschist, and chloritized eclogite, respectively. Black line represents normal mid-oceanic ridge basalt (MORB). Gray shaded region represents range of island arcs (GEOROC data; http://georoc.mpch-mainz.gwdg.de/georoc/). Yellow shaded region represents oceanic plateaus (Ontong Java, Kerguelen, Caribbean; GEOROC data). (B) Nb/La (ppm/ppm) versus K_2O (wt%). Black horizontal line represents model BSE (primitive mantle; McDonough and Sun, 1995) and corresponds to MORBs and hotspot magmas. Gray shaded region represents range for island arc basalts (Kelemen et al., 2003). LIP—large igneous province.

during reactions between eclogite and surrounding serpentinite. We note, however, that the Tian Shan retrograde eclogite series show no coupled Pb enrichments with Cr, and instead show depletions in Pb (van der Straaten et al., 2008). Assuming that reaction with serpentinite is involved in the retrogression of both the Tian Shan and Ring Mountain eclogites, these differences in Pb behavior require explanation. One speculation is that Pb mobility may be related to the different *P-T* paths undergone by these lithologies in the two regions. In the Tian Shan case, inferred *P-T* paths are clockwise, with the retrograde path showing increasing thermal gradients during exhumation (van der Straaten et al., 2008). In contrast, the Ring Mountain case shows a counterclockwise path wherein the retrograde segment follows a decreasing thermal gradient during exhumation, a feature thought to be related to refrigeration by the downgoing Farallon plate (Tsujimori et al., 2006a). Thus, one possibility is that Pb was completely mobilized out of the system in the Tian Shan case due to the higher temperatures of retrograde metamorphism (~600 °C at 1.5 GPa) compared to that seen in the Ring Mountain case (~400 °C at 1.5 GPa).

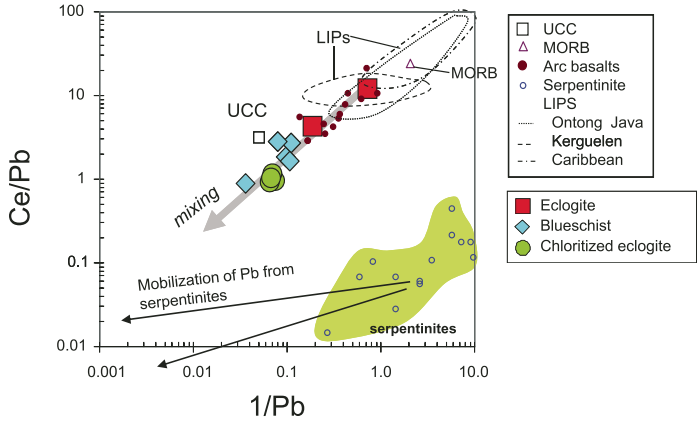

Figure 8. Ce/Pb versus 1/Pb (ppm by weight) for eclogites, blueschists, chloritized eclogites, and different reservoirs (see text and legend; MORB—mid-oceanic ridge basalt [Sun and McDonough, 1989], UCC—upper continental crust [Rudnick and Gao, 2003]; outlined regions represent large igneous provinces [LIPs] and hotspot magmas [GEOROC; http://georoc.mpch-mainz.gwdg.de/georoc/]; serpentinite data are from Li and Lee [2006]). Thick gray arrow shows mixing trajectory pointing toward a high Pb, low Ce/Pb fluid component. Green outlined region represents serpentinites. Horizontal arrows show predicted range of fluid compositions released from serpentinites.

Eclogite Exhumation via Serpentinite Channels

Our geochemical observations indicate that eclogite exhumation and retrogression were accompanied by reaction with pelitic sediments and serpentinites. The fact that the trace element signatures of retrograde blueschist envelopes and chloritized eclogites all indicate reaction with serpentinite requires that eclogite and serpentinite were juxtaposed and reacted along the entire retrograde path from high to low pressures. This suggests that the eclogites were carried up in a long serpentinite channel extending from peak metamorphic pressures to the surface. This does not rule out the possibility

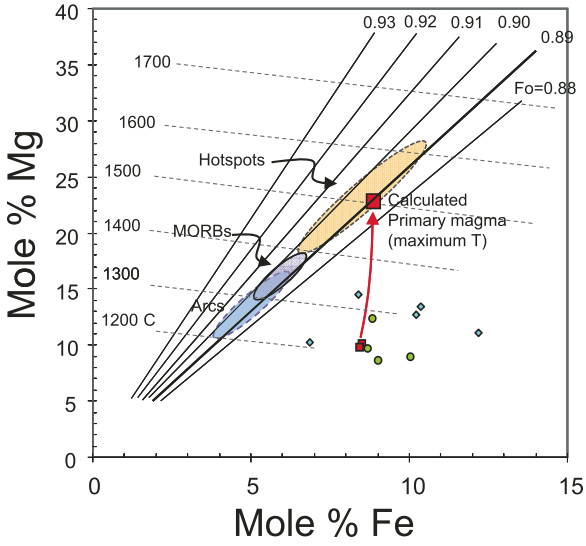

Figure 9. Cation mole percent Mg versus Fe in the eclogites, blueschists, and chloritized eclogites. Positive slope lines correspond to Mg-Fe magma compositions in equilibrium with olivine of a given forsterite [Fo = 100 * molar Mg/(Mg + Fe)] content; primary basalts should be in equilibrium with $Fo_{89–90}$. Negative slope lines correspond to temperature contours based on Fe-Mg exchange between melt and olivine (Putirka et al., 2007; Roeder and Emslie, 1970). Large red square represents inferred primary magma composition of the eclogites estimated by back-correcting for olivine fractionation (following methods described in Courtier et al., 2007); red arrow represents olivine fractionation trend. Orange oval corresponds to temperatures of hotspot and flood basalt primary magmas, and blue oval corresponds to that of mid-ocean ridges and arcs (Courtier et al., 2007; Lee et al., 2009; Leeman et al., 2005). MORB—mid-oceanic ridge basalt; T—temperature.

that the last stages of exhumation were accommodated by crustal level extension along the lines of metamorphic core complexes.

These observations and arguments are thus consistent with eclogite exhumation via serpentinite-bearing channels (Ernst, 1970; Ernst et al., 1997; Guillot et al., 2001; Moore, 1984; Schwartz et al., 2001). These serpentinite channels could represent original serpentinites within the subducting oceanic lithosphere itself, that is, just beneath the oceanic crust. Alternatively, the serpentinite channel could consist of secondary serpentinites, formed in the mantle wedge above the slab-mantle interface. Secondary serpentinite in the corner of the mantle wedge above the subducting slab are thought to form as water in pores or bound in hydrous minerals in subducted sediments and altered oceanic crust is released into the corner of the overlying mantle wedge. Serpentinized mantle wedges are the best explanations for low seismic velocity corners in the mantle wedge observed in some active subduction zones (Bostock and Van Decar, 1994).

If a serpentinite channel does exist, it could represent a convenient exhumation pathway for high-grade metamorphic rocks. Serpentinite has a much lower density than the mantle (2700 kg/m^3 compared to 3300 kg/m^3) and a very low viscosity (Hilairet et al., 2007). The former provides a strong buoyancy force generating a pressure gradient that can drive flow of the serpentinite to the surface, whereas the low viscosity reduces the viscous resisting forces (Ernst, 1970; Ernst et al., 1997; Guillot et al., 2001). Coupled with erosion of the serpentinite at the surface (e.g., via serpentinite mud volcanoes; Fryer et al., 2000), considerable upward transport along this serpentine channel may occur. As these serpentinites rise, they may disrupt eclogitized oceanic crust or seamounts, transporting such fragments to the surface. Of interest are the ascent rates of these serpentinite channels. If ascent rates are too low, the eclogites would probably undergo complete retrograde metamorphism. Retrogression kinetics would be further enhanced by the fact that the eclogites are surrounded by a hydrous matrix of serpentinites or sediments. Thus, the question is whether ascent rates within serpentinite channels are ever fast enough to match those constrained by the geochronologic studies discussed above and to prevent complete retrogression.

Ascent Rates in Serpentinite Channels and the Role of Oblique Convergence

In order to assess the physical plausibility of the serpentinite channel hypothesis, we now explore simple quantitative models of eclogite exhumation in serpentinite channels. A number of simple models of serpentinite channel flow have been presented (Guillot et al., 2001; Schwartz et al., 2001). It is important that there is a trade-off between serpentinite layer thickness and ascent rate, because the thinner the layer thickness, the greater the viscous resisting forces and the slower the ascent rate. Thus, large serpentinite layer thicknesses are needed for serpentinite ascent rates to exceed the downward dragging force associated with the subducting slab (layer thicknesses must be >10 km for a ~10 cm/yr plate velocity; Schwartz et al., 2001). However, in the case of the Franciscan eclogites at Ring Mountain, it has been suggested that the angle of subduction was initially low, possibly making it difficult to accommodate thick serpentinite channels. If the serpentinite channel hypothesis is correct, as is implied from our observations, additional physics must be explored.

In this regard, it is worth exploring the possible relationship between exhumation and obliquity of subduction. It has been suggested that exhumation of high-grade metamorphic rocks is globally related to oblique convergence (Tsujimori et al., 2006b). Eclogites in Central America, the Caribbean islands, and northern Venezuela and Ecuador all occur in serpentinite mélanges and were formed along oblique subduction margins between the Caribbean plate and North and South America (Avé Lallemant and Guth, 1990; Giaramita and Sorensen, 1994; Harlow et al., 2004). Serpentinite-hosted eclogites in Papua New Guinea also crop out along highly oblique convergence zones between the Pacific and Australian plates (Baldwin et al., 2004). As for the obliquity of Farallon–North American convergence during eclogite exhumation, there is still considerable debate. During the Jurassic and Early Cretaceous, when many of the Franciscan eclogites were formed and

exhumed, subduction is thought to have been oblique (Wakabayashi, 1992). However, it has also been suggested that effusive continental arc magmatism during the mid-Cretaceous required more normal convergence (Ernst et al., 2008).

The purpose here is not to resolve whether oblique convergence was involved in any of the above-mentioned regions where eclogite exhumation took place. Instead, we simply explore the consequences of oblique convergence in eclogite exhumation. We first assume that the eclogite bodies are small enough that they are passively carried by the serpentinite matrix. Hence, we consider only the flow of the serpentinite. The buoyancy of the serpentinite generates a pressure gradient that drives flow along a narrow channel. This pressure gradient is given by $\Delta\rho g\sin\theta$, where $\Delta\rho$ is the positive (upward) density contrast between serpentinite and mantle, g is gravitational acceleration, and θ is the dip angle of subduction (Figs. 10A, 10B). Relative to the channel, the average upward velocity of the serpentinite can be approximated by Poiseulle channel flow, and is given by:

$$V = \Delta\rho g H^2 \sin\theta/(12\eta), \qquad (3)$$

where H is the full width of the channel and η is the serpentinite viscosity. The average net velocity upward, V_{net}, however, is the difference between the upward channel velocity and the downward-sinking velocity of the plate (e.g., a Couette component). The downward-sinking velocity of the plate is given by $V_s = V_P\cos\beta$, where V_P is the relative plate velocity and β is the angle of oblique convergence (0° reflects pure normal convergence and 90° represents pure strike-slip motion).

In Figures 10C and 10D, we consider one set of variables to illustrate how the time, t, needed to return eclogites from their depths of formation ($Z_{serpentinite}$ ~50 km), i.e., $t = Z_{serp}/(V_{net}\sin\theta)$, depends on dip angle and obliqueness. We assume serpentinite to be weak ($\eta = 10^{18}$ Pa s), a density contrast $\Delta\rho$ of 500 kg/m^3, a full channel width of ~5 km, and a relative plate velocity V_P of 10 cm/yr. It can be seen that return times are shortest for high dip angles because the

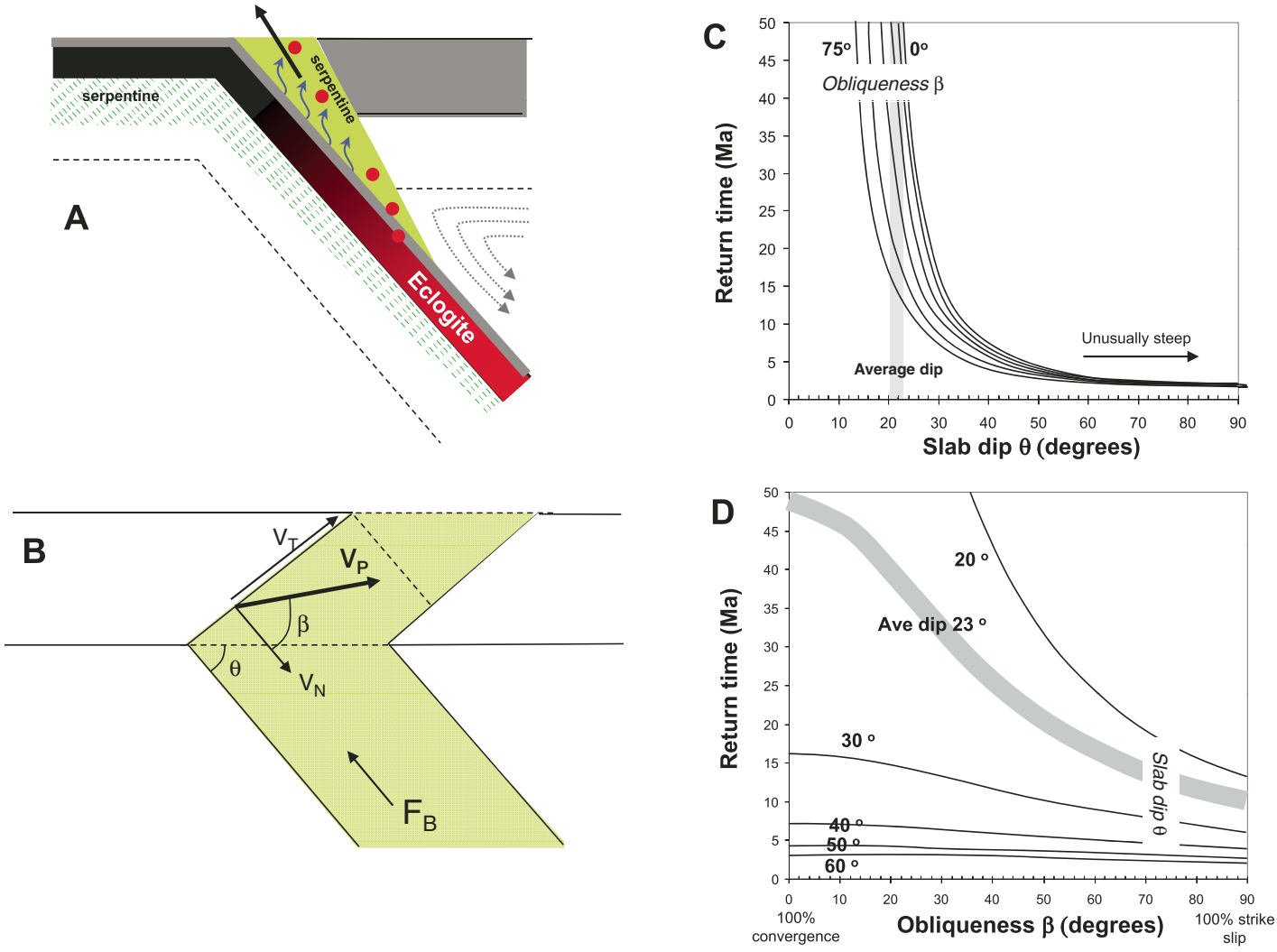

Figure 10. (A) How a serpentine channel forms in the cold corner of the mantle wedge above a subducting slab. (B) Idealized blow-up of the serpentine channel in A. Buoyant force F_B pushes serpentine up with a trench normal component. Normal component of oblique subduction resists this buoyancy. V_P is relative plate velocity, V_N is normal component, V_T is transverse component, θ is slab dip, and β is obliqueness angle. (C) Eclogite return time (Ma) versus slab dip and contoured against obliqueness angle. See text for parameters. (D) Eclogite return time versus obliqueness angle and contoured against slab dip. Ave—average.

pressure gradient is greatest and the trench-normal distance along the slab to Z_{serp} is shortest. However, high dip angles are uncommon in subduction zones (though possibly common in continent-continent collisions). We thus focus our attention on lower dips, where the model is most relevant. For example, the global average dip of subducting slabs is ~23°. At these angles, the pressure gradient driving flow is lower, so the effect of oblique convergence becomes more important. For a given dip, exhumation is most rapid (on the order of several kilometers per million years) during oblique convergence (Fig. 10D) because the downward subduction component is reduced and hence competes less with the upward channel flow of serpentinite. In the extreme case of nearly pure strike-slip motion ($\beta = 90°$), the relevance of the model breaks down because there is no subduction component to generate eclogites. Our model shows that for a given combination of plate velocity and slab dip, rapid eclogite exhumation similar to that inferred from the geochronologic studies discussed in the Introduction appears to be favored during oblique subduction. Many of the parameters in this simple model can be varied considerably, but the general physics and trends presented here will not change.

Our simple calculations shown here indicate that eclogite exhumation can occur by transport in buoyant serpentinite channels. Although not a requisite for exhumation, oblique convergence can increase ascent rates, thereby decreasing the elapsed time between peak metamorphism and exhumation. We suggest that in oblique convergence zones, eclogite ascent rates are fast enough to prevent complete retrogression of high-grade metamorphic rocks.

CONCLUSION

The Ring Mountain eclogites show petrographic evidence on their rinds for retrograde metamorphism into blueschists and greenschists. Based on major element systematics, REE abundance patterns, and Nb/Ta and Nb/La ratios, the protoliths of these mafic lithologies are consistent with tholeiitic basalts (normal MORB to enriched MORB). Retrograde lithologies show two independent styles of metasomatic enrichments, one represented by addition of LILEs (Cs, Rb, K, Ba, and Tl) and another represented by correlated enrichments of Cr, Mg, Ni, and Pb. The former are likely related to reaction with metamorphosed pelitic sediments or with fluids derived from them; the latter are best explained by reaction with serpentinites. Because all of the retrograde lithologies show the serpentinite overprint, the eclogites must have undergone reaction with serpentinite along the entire retrograde path. These observations are thus consistent with eclogite exhumation along serpentinite channels extending down to the depths of the eclogites, perhaps formed just above the slab-mantle wedge interface by the infiltration of dehydrating fluids from the subducting slab. Simple models show that the low viscosity and low density of serpentinite are sufficient to drive the upward flow of serpentinite. However, the rapid ascent rates needed to return eclogites to the surface without complete retrograde metamorphism are most easily attained in oblique subduction zone settings.

ACKNOWLEDGMENTS

Grants from the National Science Foundation and the Packard Foundation supported this research. This work constitutes part of Horodyskyj's undergraduate research projects at Rice University. The comments of two anonymous reviewers, and discussions with A. Basu, S. Sorensen, J. Wakabayashi, and J. Platt are appreciated. We especially thank W.G. Ernst and H. Avé Lallemant for the generous donation of their time and discussions. We also thank R. Halama for bringing to our attention the work on retrograde eclogites in the Tian Shan.

REFERENCES CITED

Ague, J.J., 2003, Fluid infiltration and transport of major, minor, and trace elements during regional metamorphism of carbonate rocks, Wepawaug Schist, Connecticut, USA: American Journal of Science, v. 303, p. 753–816, doi: 10.2475/ajs.303.9.753.

Ague, J.J., and van Haren, J.L.M., 1996, Assessing metasomatic mass and volume changes using the bootstrap, with application to deep crustal hydrothermal alteration of marble: Economic Geology and the Bulletin of the Society of Economic Geologists, v. 91, p. 1169–1182.

Anczkiewicz, R., Platt, J.P., Thirlwall, M.F., and Wakabayashi, J., 2004, Franciscan subduction off to a slow start: Evidence from high-precision Lu-Hf garnet ages on high-grade blocks: Earth and Planetary Science Letters, v. 225, p. 147–161, doi: 10.1016/j.epsl.2004.06.003.

Avé Lallemant, H.G., and Guth, L.R., 1990, Role of extensional tectonics in exhumation of eclogites and blueschists in an oblique subduction setting; northeastern Venezuela: Geology, v. 18, p. 950–953, doi: 10.1130/0091-7613(1990)018<0950:ROETIE>2.3.CO;2.

Baldwin, S.L., Monteleone, B.D., Webb, L.E., Fitzgerald, P.G., Grove, M., and Hill, E.J., 2004, Pliocene eclogite exhumation at plate tectonic rates in eastern Papua New Guinea: Nature, v. 431, p. 263–267, doi: 10.1038/nature02846.

Bebout, G.E., 2007, Metamorphic chemical geodynamics of subduction zones: Earth and Planetary Science Letters, v. 260, p. 373–393, doi: 10.1016/j.epsl.2007.05.050.

Bebout, G.E., and Barton, M.D., 2002, Tectonic and metasomatic mixing in a high-T, subduction-zone melange—Insights into the geochemical evolution of the slab-mantle interface: Chemical Geology, v. 187, p. 79–106, doi: 10.1016/S0009-2541(02)00019-0.

Bostock, M.B., and Van Decar, J.C., 1994, Upper mantle structure of the northern Cascadia subduction zone: Canadian Journal of Earth Sciences, v. 32, p. 1–12.

Brimhall, G.H., and Dietrich, W.E., 1987, Constitutive mass balance relations between chemical composition, volume, density, porosity, and strain in metasomatic hydrochemical systems: Results on weathering and pedogenesis: Geochimica et Cosmochimica Acta, v. 51, p. 567–587, doi: 10.1016/0016-7037(87)90070-6.

Catlos, E.J., and Sorensen, S.S., 2003, Phengite-based chronology of K- and B-rich fluid flow in two paleo-subduction zones: Science, v. 299, p. 92–95, doi: 10.1126/science.1076977.

Cloos, M., 1985, Thermal evolution of convergent plate margins: Thermal modeling and reevaluation of isotopic Ar-ages for blueschists in the Franciscan complex of California: Tectonics, v. 4, p. 421–433, doi: 10.1029/TC004i005p00421.

Courtier, A.M., and 14 others, 2007, Correlation of seismic and petrologic thermometers suggests deep thermal anomalies beneath hotspots: Earth and Planetary Science Letters, v. 264, p. 308–316, doi: 10.1016/j.epsl.2007.10.003.

Ernst, W.G., 1970, Tectonic contact between the Franciscan mélange and the Great Valley sequence—Crustal expression of a late Mesozoic Benioff zone: Journal of Geophysical Research, v. 75, p. 886–901, doi: 10.1029/JB075i005p00886.

Ernst, W.G., Maruyama, S., and Wallis, S., 1997, Buoyancy-driven, rapid exhumation of ultrahigh-pressure metamorphosed continental crust: National Academy of Sciences Proceedings, v. 94, p. 9532–9537, doi: 10.1073/pnas.94.18.9532.

Ernst, W.G., Snow, C.A., and Scherer, H.H., 2008, Mesozoic transpression, transtension, subduction and metallogenesis in northern and central California: Terra Nova, v. 20, p. 394–413, doi: 10.1111/j.1365-3121.2008.00834.x.

Fryer, P., Lockwood, J.P., Becker, N., Phipps, S., and Todd, C.S., 2000, Significance of serpentine mud volcanism in convergent margins, *in* Dilek, Y., Moores, E., Elthon, D., and Nicolas, A., eds., Ophiolites and oceanic crust: New insights from field studies and the Ocean Drilling Program: Geological Society of America Special Paper 349, p. 35–51.

Giaramita, M.J., and Sorensen, S.S., 1994, Primary fluids in low-temperature eclogites: Evidence from two subduction complexes (Dominican Republic, and California, USA): Contributions to Mineralogy and Petrology, v. 117, p. 279–292, doi: 10.1007/BF00310869.

Godard, M., Kelemen, P.B., Hart, S.H., Jackson, M., and Hanghoj, K., 2005, High Pb/Ce reservoir in depleted altered mantle peridotites: Eos (Transactions, American Geophysical Union), v. 86, p. F1937.

Guillot, S., Hattori, K.H., de Sigoyer, J., Nagler, T., and Auzende, A.-L., 2001, Evidence of hydration of the mantle wedge and its role in the exhumation of eclogites: Earth and Planetary Science Letters, v. 193, p. 115–127, doi: 10.1016/S0012-821X(01)00490-3.

Harlow, G.E., Hemming, S.R., Avé Lallemant, H.G., Sisson, V.B., and Sorensen, S.S., 2004, Two high-pressure-low-temperature serpentinite-matrix mélange belts, Moagua fault zone, Guatemala: A record of Aptian and Maastrichtian collisions: Geology, v. 32, p. 17–20, doi: 10.1130/G19990.1.

Herzberg, C., Asimow, P.D., Arndt, N.T., Niu, Y., Lesher, C.M., Fitton, J.G., Cheadle, M.J., and Saunders, A.D., 2007, Temperatures in ambient mantle and plumes: Constraints from basalts, picrites and komatiites: Geochemistry Geophysics Geosystems, v. 8, p. doi:10.1029/2006GC001390.

Hilairet, N., Reynard, B., Wang, Y., Daniel, I., Merkel, S., Nishiyama, N., and Petitgirard, S., 2007, High-pressure creep of serpentine, interseismic deformation, and initiation of subduction: Science, v. 318, p. 1910–1913.

Hofmann, A.W., 1988, Chemical differentiation of the Earth: The relationship between mantle, continental crust, and oceanic crust: Earth and Planetary Science Letters, v. 90, p. 297–314, doi: 10.1016/0012-821X(88)90132-X.

Hofmann, A.W., 1997, Mantle geochemistry: the message from oceanic volcanism: Nature, v. 385, p. 219–229, doi: 10.1038/385219a0.

Hofmann, A.W., Jochum, K.P., Seufert, M., and White, W.M., 1986, Nb and Pb in oceanic basalts: New constraints on mantle evolution: Earth and Planetary Science Letters, v. 79, p. 33–45, doi: 10.1016/0012-821X(86)90038-5.

Kelemen, P.B., Hanghoj, K., and Greene, A.R., 2003, One view of the geochemistry of subduction-related magmatic arcs, with an emphasis on primitive andesite

and lower crust, *in* Rudnick, R.L., ed., Treatise on geochemistry, Volume 3: Amsterdam, Elsevier, p. 593–659, doi: 10.1016/B0-08-043751-6/03035-8.

Kelemen, P.B., Johnson, K.T.M., Kinzler, R.J., and Irving, A.J., 1990, High-field-strength element depletions in arc basalts due to mantle-magma interaction: Nature, v. 345, p. 521–524, doi: 10.1038/345521a0.

Kelemen, P.B., Kikawa, E., Miller, D.J., and the Shipboard Scientific Party, 2007, Leg 209 Summary: Processes in a 20-km-thick conductive boundary layer beneath the Mid-Atlantic ridge, 14°–16° N, *in* Kelemen, P.B., et al., Proceedings of the Ocean Drilling Program, Scientific results, Volume 209: College Station, Texas, Ocean Drilling Program, p. 1–33, doi: 10.2973/odp.proc.sr.209.001.2007.

Lee, C.-T.A., 2005, Trace element evidence for hydrous metasomatism at the base of the North American lithosphere and possible association with Laramide low-angle subduction: Journal of Geology, v. 113, p. 673–685, doi: 10.1086/449327.

Lee, C.-T.A., Luffi, P., Plank, T., Dalton, H.A., and Leeman, W.P., 2009, Constraints on the depths and temperatures of basaltic magma generation on Earth and other terrestrial planets using new thermobarometers for mafic magmas: Earth and Planetary Science Letters, v. 279, p. 20–33, doi: 10.1016/j.epsl.2008.12.020.

Leeman, W.P., Lewis, J.F., Evarts, R.C., Conrey, R.M., and Streck, M.J., 2005, Petrologic constraints on the thermal structure of the southern Washington Cascades: Journal of Volcanology and Geothermal Research, v. 140, p. 67–105, doi: 10.1016/j.jvolgeores.2004.07.016.

Li, Z.X.A., and Lee, C.-T.A., 2006, Geochemical investigation of serpentinized oceanic lithospheric mantle in the Feather River Ophiolite, California: Implications for the recycling rate of water by subduction: Chemical Geology, v. 235, p. 161–185, doi: 10.1016/j.chemgeo.2006.06.011.

Little, M.G., and Lee, C.-T.A., 2006, On the formation of an inverted weathering profile on Mount Kilimanjaro, Tanzania: Buried paleosol or groundwater weathering?: Chemical Geology, v. 235, p. 205–221, doi: 10.1016/j.chemgeo.2006.06.012.

McDonough, W.F., and Sun, S.S., 1995, The composition of the Earth: Chemical Geology, v. 120, p. 223–253, doi: 10.1016/0009-2541(94)00140-4.

Moore, D.E., 1984, Metamorphic history of a high-grade blueschist exotic block from the Franciscan Complex, California: Journal of Petrology, v. 25, p. 126–150.

Niu, Y., 2004, Bulk-rock major and trace element compositions of abyssal peridotites: Implications for mantle melting, melt extraction and post-melting processes beneath mid-ocean ridges: Journal of Petrology, v. 45, p. 2423–2458, doi: 10.1093/petrology/egh068.

Platt, J.P., 1975, Metamorphic and deformational processes in the Franciscan complex, California: Some insights from the Catalina Schist terrane: Geological Society of America Bulletin, v. 86, p. 1337–1347, doi: 10.1130/0016-7606(1975)86<1337:MADPIT>2.0.CO;2.

Platt, J.P., 1986, Dynamics of orogenic wedges and the uplift of high-pressure metamorphic rocks: Geological Society of America Bulletin, v. 97, p. 1037–1053, doi: 10.1130/0016-7606(1986)97<1037:DOOWAT>2.0.CO;2.

Platt, J.P., 1993, Exhumation of high-pressure rocks: A review of concepts and processes: Terra Nova, v. 5, p. 119–133, doi: 10.1111/j.1365-3121.1993.tb00237.x.

Putirka, K.D., Perfit, M., Ryerson, F.J., and Jackson, M.G., 2007, Ambient and excess mantle temperatures, olivine thermometry, and active vs. passive upwelling: Chemical Geology, v. 241, p. 177–206, doi: 10.1016/j.chemgeo.2007.01.014.

Roeder, P.L., and Emslie, R.F., 1970, Olivine-liquid equilibrium: Contributions to Mineralogy and Petrology, v. 29, p. 275–289, doi: 10.1007/BF00371276.

Rudnick, R.L., and Gao, S., 2003, Composition of the continental crust, *in* Rudnick, R.L., ed., Treatise on geochemistry, Volume 3: Amsterdam, Elsevier, p. 1–64, doi: 10.1016/B0-08-043751-6/03016-4.

Saha, A., Basu, A.R., Wakabayashi, J., and Wortman, G.L., 2005, Geochemical evidence for subducted infant arc in Franciscan high-grade tectonic blocks: Geological Society of America Bulletin, v. 117, p. 1318–1335, doi: 10.1130/B25593.1.

Schemmann, K., Unruh, J.R., and Moores, E.M., 2008, Kinematics of Franciscan Complex exhumation: New insights from the geology of Mount Diablo, California: Geological Society of America Bulletin, v. 120, p. 543–555, doi: 10.1130/B26056.1.

Schwartz, S., Allemand, P., and Guillot, S., 2001, Numerical model of the effect of serpentinites on the exhumation of eclogitic rocks: Insights from the Monviso ophiolitic massif (western Alps): Tectonophysics, v. 342, p. 193–206, doi: 10.1016/S0040-1951(01)00162-7.

Sorensen, S.S., and Grossman, J.N., 1989, Enrichment of trace elements in garnet amphibolites from a paleosubduction zone: Catalina Schist, southern California: Geochimica et Cosmochimica Acta, v. 53, p. 3155–3177, doi: 10.1016/0016-7037(89)90096-3.

Sun, S.S., and McDonough, W.F., 1989, Chemical and isotopic systematics of oceanic basalts: implications for mantle composition and processes, *in* Saunders, A.D., and Norry, M.J., eds., Magmatism in ocean basins: Geological Society of London Special Publication 42, p. 313–345.

Tsujimori, T., Matsumoto, K., Wakabayashi, J., and Liou, J.G., 2006a, Franciscan eclogite revisited: Reevaluation of the P-T evolution of tectonic blocks from Tiburon Peninsula, California, USA: Mineralogy and Petrology, v. 88, p. 243–267, doi: 10.1007/s00710-006-0157-1.

Tsujimori, T., Sisson, V.B., Liou, J.G., Harlow, G.E., and Sorensen, S.S., 2006b, Very-low-temperature record of the subduction process: A review of worldwide lawsonite eclogites: Lithos, v. 92, p. 609–624, doi: 10.1016/j.lithos.2006.03.054.

van der Straaten, F., Schenk, V., John, T., and Gao, J., 2008, Blueschist-facies rehydration of eclogites (Tian Shan, NW-China): Implications for fluid-rock interaction in the subduction channel: Chemical Geology, v. 255, p. 195–219, doi: 10.1016/j.chemgeo.2008.06.037.

Wakabayashi, J., 1992, Nappes, tectonics of oblique plate convergence, and metamorphic evolution related to 140 million years of continuous subduction, Franciscan complex, California: Journal of Geology, v. 100, p. 19–40, doi: 10.1086/629569.

Manuscript Received 10 February 2009
Revised Manuscript Received 10 July 2009
Manuscript Accepted 23 July 2009